

The role of hERG1 ion channels in epithelial-mesenchymal transition and the capacity of riluzole to reduce cisplatin resistance in colorectal cancer cells

Angelo Fortunato^{1,2}

Accepted: 11 May 2017 / Published online: 7 June 2017
© International Society for Cellular Oncology 2017

Abstract

Purpose The transition of cells from the epithelial to the mesenchymal state (EMT) plays an important role in tumor progression. EMT allows cells to acquire mobility, stem-like behavior and resistance to apoptosis and drug treatment. These features turn EMT into a central process in tumor biology. Ion channels are attractive targets for the treatment of cancer since they play critical roles in controlling a wide range of physiological processes that are frequently deregulated in cancer. Here, we investigated the role of ether-a-go-go-related 1 (hERG1) ion channels in the EMT of colorectal cancer cells. **Methods** We studied the epithelial-mesenchymal profile of different colorectal cancer-derived cell lines and the expression of hERG1 potassium channels in these cell lines using real-time PCR. Next, we knocked down hERG1 expression in HCT116 cells using lentivirus mediated RNA interference and characterized the hERG1 silenced cells in vitro and in vivo. Finally, we investigated the capacity of riluzole, an ion channel-modulating drug used in humans to treat amyotrophic lateral sclerosis, to reduce the resistance of the respective colorectal cancer cells to the chemotherapeutic drug cisplatin. **Results** We found that of the colorectal cancer-derived cell lines tested, HCT116 showed the highest mesenchymal profile and a high hERG1 expression. Subsequent hERG1

expression knockdown induced a change in cell morphology, which was accompanied by a reduction in the proliferative and tumorigenic capacities of the cells. Notably, we found that hERG1 expression knockdown elicited a reversion of the EMT profile in HCT116 cells with a reacquisition of the epithelial-like profile. We also found that riluzole increased the sensitivity of HCT116 cisplatin-resistant cells to cisplatin. **Conclusions** Our data indicate that hERG1 plays a role in the EMT of colorectal cancer cells and that its knockdown reduces the proliferative and tumorigenic capacities of these cells. In addition, we conclude that riluzole may be used in combination with cisplatin to reduce chemo-resistance in colorectal cancer cells.

Keywords EMT · hERG1 · RNAi · ion channels · colorectal cancer · riluzole · cisplatin

1 Introduction

Colorectal cancer is a heterogeneous disorder and there is no specific molecular profile that characterizes this disorder [1, 2]. Unsupervised gene expression analysis of colorectal cancer has, however, indicated that the epithelial-mesenchymal transition (EMT) signature may be correlated with a poor survival of the patients [3]. EMT is a cellular process that is characterized by molecular and morphological changes through which epithelial cells acquire features of mesenchymal cells. EMT is involved in the differentiation of tissues, in organ development and in tissue repair, but it can also adversely contribute to disease development such as cancer [4–6]. EMT allows carcinoma cells to acquire stem cell-like characteristics, motility and invasiveness, as well as resistance to apoptosis and chemoresistance. Therefore, EMT is thought to contribute significantly to tumor progression and the

Electronic supplementary material The online version of this article (doi:10.1007/s13402-017-0328-6) contains supplementary material, which is available to authorized users.

✉ Angelo Fortunato
afortun2@asu.edu

¹ Department of Experimental and Clinical Biomedical Sciences, University of Florence, Florence, Italy

² Biodesign Center for Personalized Diagnostic, Arizona State University, PO Box 875001, Tempe, AZ 85287-5001, USA

metastatic behavior of cancer cells [7–12]. A number of genes associated with EMT has been identified [13, 14], but the role of ion channels, in particular potassium channels, has so far not adequately been addressed.

Potassium channels constitute a large class of ion channels that are involved in several physiological processes. K^+ channels contribute to regulation of the membrane potential, cell volume and intracellular pH changes during cell cycle progression [15]. They are abundantly expressed in excitable cells [16] and are often aberrantly expressed in cancer cells in which they contribute to the regulation of several aspects of cellular behavior such as evasion of apoptosis, proliferation, angiogenesis, tissue invasion and metastasis [17–20]. Blocking of K^+ channels has been found to elicit anti-neoplastic activities in different types of cancer [21].

Interestingly, a profound reorganization of plasma membrane ion channels has been found to occur in meta-nephrogenic mesenchymal-epithelial transition (MET) during kidney development [22]. There are also several reports suggesting an involvement of ion channels in the EMT of cancer cells. It has, for instance, been found that Ca^{2+} influx contributes to the regulation of EMT in human breast cancer cells [23, 24] and that the expression of EAG1 (KCNH1) K^+ channels, after treatment with TGF β 1, is up-regulated during EMT in lung cancer cells [25], suggesting an involvement of these channels in cancer EMT [26]. In particular, it has been found that hERG1 (KCNH2) K^+ channels are over-expressed in several types of cancer, including colorectal adenocarcinoma [3]. hERG1 channels in cancer cells can form macromolecular complexes with integrin receptors [27] and it has been found that these protein-protein interactions play a role in modulating adhesive interactions of cells with the extracellular matrix, thereby promoting cell motility and invasiveness. In addition, it has been found that integrin-hERG1 channel complexes can regulate downstream signaling pathways [27].

Since they play a critical role in controlling a wide range of physiological processes and are often deregulated in cancer, ion channels may serve as attractive drug targets for the treatment of cancer [28, 29]. Here, we characterized the role of hERG1 K^+ channels in EMT using HCT116 colorectal cancer-derived cells as a model and we investigated the capacity of riluzole, an ion channel-modulating drug used in humans to treat amyotrophic lateral sclerosis [30, 31], to reduce the resistance of these cells to the chemotherapeutic drug cisplatin.

2 Materials and methods

2.1 hERG1 lentivirus mediated RNA interference

We used lentivirus vectors to transduce colorectal cancer cells with shRNA constructs capable of post-transcriptionally silencing specific genes. Each shRNA construct (commercially

distributed by Open Biosystems) included a hairpin of 21 base pairs, a sense and antisense stem and a 6 base pair loop cloned into a pLKO.1 lentiviral vector harboring a puromycin resistance gene. When the shRNA molecules are processed by cellular enzymes they become activated (siRNA), ultimately leading to degradation of the complementary mRNAs by the RNA interference machinery. In order to preliminarily test the effectiveness of the shRNA, HCT116 cells were transfected using Lipofectamine® 2000 Transfection Reagent (Invitrogen™) according to the manufacturer's instructions. Next, we produced lentivirus particles by co-transfecting 2nd generation lentiviral plasmids and the transfer vector construct into HEK293T packaging cells. Successively, we transduced colorectal cancer-derived HCT116 cells with virus at a multiplicity of infection (MOI) = 3 and 5. Subsequently, we selected stable silenced cell lines using puromycin.

2.2 Cell lines and growth assays

The colorectal cancer-derived cell lines HCT116, H630, HCT8, CACO2 and HT29 were purchased from the American Type Culture Collection (ATCC) (Rockville, MD, USA). HCT116, H630 and HCT8 cells were grown in RPMI-1640 medium (EuroClone), CACO2 cells in DMEM medium (EuroClone) and HT29 cells in McCoy's medium (EuroClone), respectively, supplemented with 2% L-Glut, 10% fetal bovine serum (FBS) (Hyclone) and 1% penicillin/streptomycin at 37 °C in a humidified 5% CO₂ atmosphere.

For soft agar colony forming assays, a bottom layer of 0.5% low melting agarose in RPMI-1640 medium, supplemented with 2% L-glu and 10% FBS, was prepared in 60 mm dishes. After solidification of the bottom layer, cells were added in RPMI-1640 culture medium containing 0.35% agarose, 2% L-glu, 10% FBS, 1% penicillin/streptomycin and puromycin (1.5 μ g/ μ l). Next, the dishes were incubated for 15 days at 37 °C in a humidified 5% CO₂ atmosphere. The experiments were performed in triplicate for each cell line used. Pictures were taken for measurement of the diameter of the colonies.

To estimate the growth rate of the different cell lines overtime, 5×10^3 cells of the respective control and experimental cell lines were seeded in 6-well plates. From a subset of wells the cells were detached and counted every day for six consecutive days.

To investigate whether the cell cycle was effected by hERG1 silencing, 3×10^5 cells were seeded in 35 mm multi-well plates in RPMI-1640 medium supplemented with 2% L-glu, puromycin (1.5 μ g/ μ l) and 10% FBS. After 24 h the cells were washed with PBS after which fresh medium without serum was added to synchronize the cell cycle. After 6, 18, 24, 30 and 72 h the cells were washed in PBS and stained with propidium iodide (PI, Sigma-Aldrich) in the presence of TRITON. Subsequently, the cells were detached from the plates using a scraper, collected in polystyrene tubes and incubated at 4 °C for 30 min. Finally, cell cycle analyses were

carried out using a cytofluorimeter. Each analysis was performed twice.

2.3 In vivo experiments

2×10^6 cells (pLKO.1 and sh7, see below) resuspended in 100 μ l culture medium were injected into the flanks of nu/nu nude mice. Each mouse was injected in one flank with control cells and in the other flank with silenced cells. Subsequent tumor development was monitored for 18 days. These in vivo experiments were carried out in accordance with the UE Directive 2010/63/EU for animal experiments.

2.4 Protein extraction and Western blotting

Total protein extraction from control and silenced cells and subsequent Western blot analyses were carried out using standard methods. Briefly, cells were lysed in cold Tris HCl (50 mM), NaCl (125 mM), NP40 (0.1%), EDTA (5 mM), NaF (0.1 M) buffer supplemented with protease inhibitors (Roche). Protein samples were loaded in SDS-PAGE gels and blotted. The resulting membranes were incubated with an anti-hERG1 COOH-terminus antibody (1:1000, Dival) and an anti-tubulin antibody (1:500, Sigma Aldrich) as described by Lastraioli et al. [32]. The hERG1 protein contains 1159 amino acids, has a molecular mass of 127 kDa and is expressed in HCT116 cells [32]. Densitometric analyses were performed on scanned films using a grey scale mode. ImageJ was used to quantify the density and size of the bands. The background near each band was subtracted. The hERG1 levels were normalized against tubulin levels [32].

2.5 Patch-clamp recording

Cells were seeded in 35 mm Petri dishes after which traces were recorded with the amplifier Axopatch 700 A tool (Molecular Devices) using whole cell configuration. I_{hERG} measurements were performed by voltage clamp according to Schönherr et al. [33].

2.6 Real time PCR analysis

Cells and tissue specimens were homogenized in TRIzol® Reagent (Invitrogen™) to isolate total RNA according to the manufacturer's protocol. The RNA integrity was assessed on an Agilent 2100 Bioanalyzer. 1 μ g total RNA of each specimen was retrotranscribed using random primers and SuperScript™ II Reverse Transcriptase (Invitrogen™) according to the manufacturer's protocol. A SYBR green fluorescent dye (Power SYBR® Green, PCR master mix, Applied Biosystems) was used to monitor DNA synthesis.

In order to validate the efficiency of the primers a 10-fold serial dilution of the cDNA was used to generate a linear

regression equation for all the genes analyzed. All the primer pairs used were found to have a correlation coefficient > 0.99 and a slope coefficient between 3.10 and 3.60, demonstrating an optimal efficiency of the primers. The slope coefficients were used to calculate the efficiency parameters. Efficiency values were used to calculate the expression of both target and control genes. Relative expression values for each gene were expressed as a ratio of the target gene expression level to the *GAPDH* gene expression level in the same sample and normalized for the level of expression of one of the samples [34, 35]. The primers for the genes of interest were designed using the software Primer3 tool (<http://frodo.wi.mit.edu/>), or were selected from the literature (Table 1S).

2.7 Chemicals

Riluzole (Sigma-Aldrich) was dissolved in DMSO at a concentration of 5 mM and cisplatin (Sigma-Aldrich) was dissolved in bi-distilled water at the concentration of 8.3 mM. Stock solutions of riluzole and cisplatin were stored at -20°C . Immediately before use the drugs were diluted to the required concentrations.

2.8 Flow cytometry analysis

Four colorectal cancer-derived cell lines were tested for their sensitivity to cisplatin: HCT116, HCT8, H630 and HT29 by flow cytometry. To this end, 1.5×10^5 cells were seeded in 6-well plates (Costar, Corning). After 24 h the cells were treated with 3 different concentrations of cisplatin (50, 100 and 150 μ M) for 24 h after which apoptotic, necrotic, dead and living cells were detected by FACSCanto flow cytometry (Becton Dickinson) using an Annexin-V-FLUOS staining kit (Roche). The sensitivity to cisplatin of hERG1 silenced cells (sh7) and pLKO.1 cells (control) was tested at different concentrations (22,5 μ g/ml, 37,5 μ g/ml, 52,5 μ g/ml, 67,5 μ g/ml, 82,5 μ g/ml, 97,5 μ g/ml) for 24 h in both adherent cells and non-adherent cells in the supernatant.

At the end of the treatment, the cells of each sample were harvested and resuspended in 500 μ l phosphate buffered saline and stained with PI (P4170, Sigma-Aldrich), a fluorescent dye that only penetrates compromised cell membranes to detect necrotic/dead cells by flow cytometry. A total of 1×10^4 cells for each sample was analyzed by FACSCanto flow cytometry (Becton Dickinson). Aggregates and debris were excluded. The percentage of PI positive cells was recorded.

2.9 Cell viability assay

Cell viability in response to drug treatment was measured using WST-1 (Roche) reagent. 10^4 cells were seeded in a 96-well plate (Costar, Corning) with 200 μ l growth medium. Next, the medium was replaced by drug-containing medium or drug-free

medium (control) and 24 h after treatment the medium was replaced by 100 μ l fresh medium per well containing 10% WST-1. After this, the cells were incubated for 20 min and the absorbance of each sample was measured using a microplate reader (ELx 800) at a wavelength of 450 nm every 20 min.

To evaluate the IC₅₀ of each drug, cells were exposed to increasing concentrations of cisplatin, riluzole or DMSO (1 μ M, 12.5 μ M, 25 μ M, 55 μ M, 85 μ M, 115 μ M, 175 μ M). All experiments were performed at least in triplicate. The IC₅₀ values were calculated using the Origin software tool.

Finally we investigated whether the combination of cisplatin and riluzole may have a synergic, additive or antagonistic effect using the Calcsyn software tool (version 2, Biosoft). This analysis was based on the combination index (CI) method described by Chou and Talahay [36]. CI = 1 indicates an additive effect, CI < 1 indicates a synergistic effect and CI > 1 indicates an antagonistic effect. The experiments were conducted following the diagonal constant ratio combination design proposed by Chou and Talalay [36]. We treated the cells with a mixture of the two drugs at their IC₅₀ concentrations with a 2-fold serial dilution (1/2, 1/4, 1/8, 1/16, 1/32, 1/64) of the IC₅₀s.

3 Results

3.1 Generation and characterization of *hERG1* silenced HCT116 cells

In order to investigate the role of *hERG1* K⁺ channels in EMT in colorectal cancer, we first screened 5 colorectal cancer-derived cell lines to identify those with a high *hERG1* expression as well as an overt mesenchymal phenotype. To define the epithelial-mesenchymal profile we measured the expression of several EMT markers: vimentin (VIM), E-cadherin (CDH1), N-cadherin (CDH2), matrix metalloproteinase 1 (MMP1), mesenchyme forkhead 1 (FOXC2) and occludin (OCLN) by the cell lines. In doing so, we found that the HCT116 cell line had the highest mesenchymal phenotype among the cell lines tested (Fig. 1) and expressed the *hERG1* gene at a relatively high level. Hence, we selected this cell line as experimental model to investigate the role of *hERG1* in EMT. To this end, we transduced HCT116 cells with shRNA constructs capable of post-transcriptionally silencing the *hERG1* gene using a lentiviral vector. Five different shRNA constructs were available for this gene. After evaluating by real time PCR the expression knock-down capacity of each shRNA, the most effective shRNAs (named sh4 and sh7) were selected for further experiments (Table 2S, Fig. 1S). Subsequently, we produced lentiviral particles by co-transfecting second generation lentiviral plasmids and the transfer vector constructs into HEK293T packaging cells. Next, we transduced HCT116 cells at MOI (Multiple Optimal Infection) = 3 and 5 and applied puromycin selection to generate stable silenced cell lines (named sh4 and sh7) and control cell

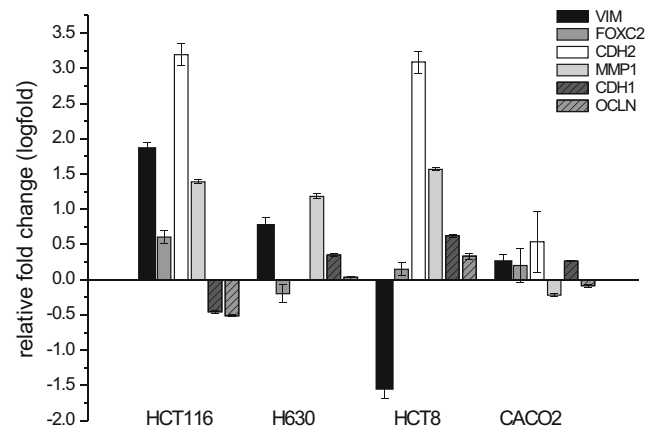


Fig. 1 EMT status of colorectal cancer-derived cell lines. High expression of mesenchymal (VIM, FOXC2, CDH2, MMP1) and low expression of epithelial (CDH1, OCLN) markers in HCT116 cells. Among the HCT116, HCT8, CACO2 and H630 cell lines tested, HCT116 cells exhibit the strongest mesenchymal profile. Relative gene expression values are expressed as ratios to that of GAPDH in the same sample and are normalized to that in HT29 cells. Histograms represent the mean (log fold) \pm s.e.m. (error bars)

lines (named pLKO.1). Analysis of *hERG1* transcription and protein expression levels (Fig. 2a, b) revealed a significant reduction of both levels in the sh4 and sh7 cell lines compared to the pLKO.1 cell line. The two silenced cell lines exhibited different *hERG1* knockdown levels, i.e., the sh4 cell line showed a more pronounced *hERG1* expression knockdown.

Next, we found by electrophysiological measurements that the silenced cells exhibited reduced *hERG1* K⁺ currents (χ^2 test, pLKO.1 (control) versus sh7 cells, $p = 0.014$; pLKO.1 (control) versus sh4, $p = 0.023$) (Fig. 2c, d). Moreover, we found that the density (pA/pF) of *hERG1* K⁺ currents was decreased in the silenced cells (mean: pLKO.1 = 2.9 ± 0.44 s.e.m., sh7 = 1.75 ± 0.20 s.e.m.; t-test, $p = 0.025$, DF = 22). Additional electrophysiological measurements of capacitance indicated a reduction in cell volume of the silenced cells (mean: pLKO.1 = 74.78 ± 7.20 s.e.m., $n = 15$, sh7 = 35.88 ± 5.40 s.e.m., $n = 15$, Mann-Whitney test $p < 0.001$). Based on these data, we conclude that *hERG1* gene expression silencing not only reduced the *hERG1* transcript and protein levels, but most importantly, also its physiological channel functions.

Since the sh7 cell line, despite a minor knockdown of the *hERG1* transcript and protein levels, exhibited a strong functional impairment of the K⁺ channel (Fig. 2c, d), we selected this cell line for assessing morphological and other biological changes. We found that the silenced cells showed a different morphology compared to the control cells (Fig. 3a, b). Particularly, we found that the silenced cells appeared to have a reduced number of membrane protrusions, making the morphology of cells more flattened, and that the cells formed cohesive groups (Fig. 3b). We also set out to investigate the tumorigenic capacity of the silenced cells using a soft agar colony formation assay. We found that the silenced cells formed smaller colonies compared to the

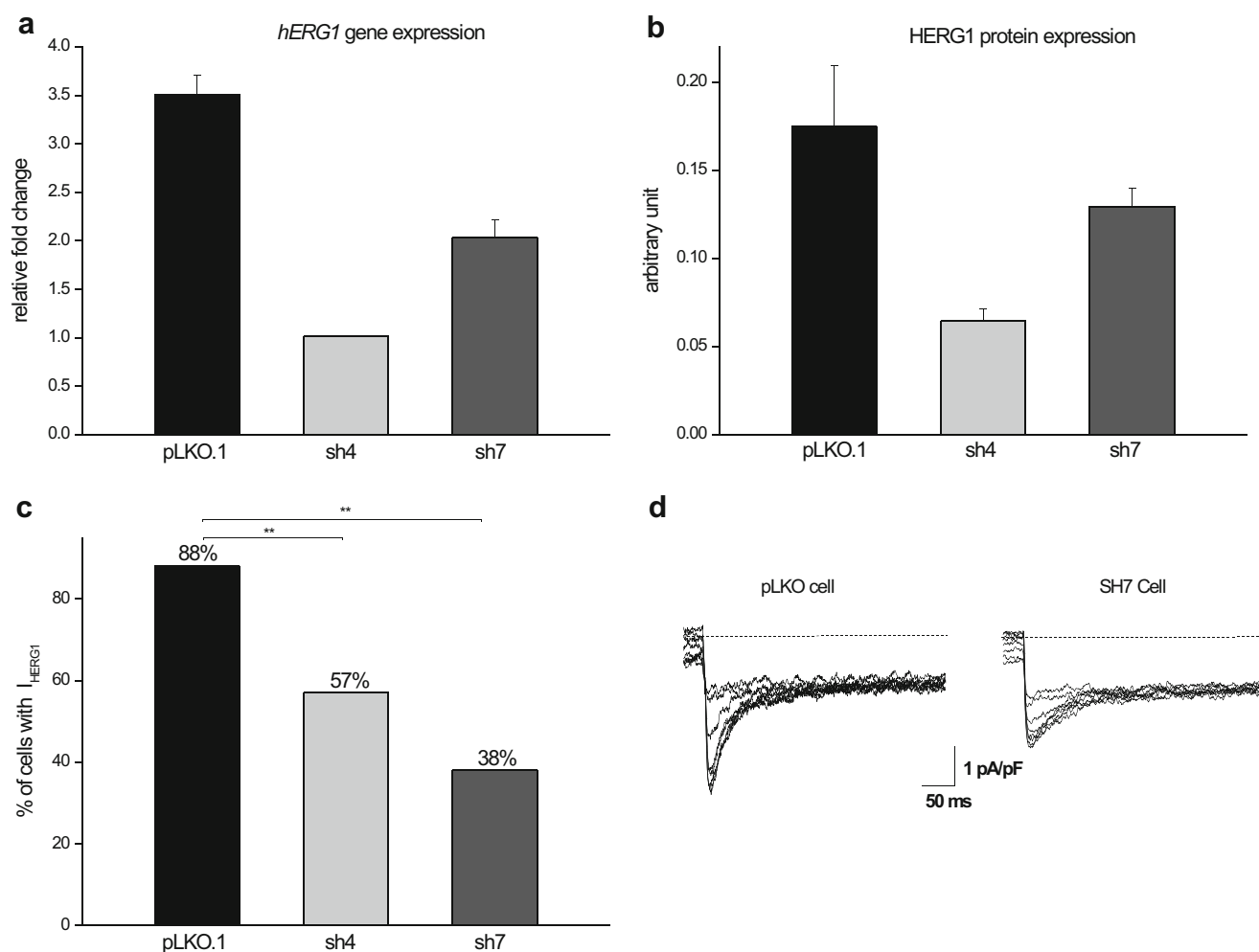


Fig. 2 Validation of hERG1 expression knockdown and its physiological consequences. **(a)** hERG1 transcript and protein **(b)** expression levels are strongly reduced by RNAi (pLKO.1: control cells transduced with the empty pLKO.1 vector; sh4 and sh7: silenced cell lines transduced with two distinct shRNAs). **(c, d)** Electrophysiological measurements (whole-

cell clamp) showing that the physiological function of the hERG1 ion channels is strongly impaired in both silenced cell lines. **(c)** Percentage of cells with hERG1 channel currents. **(d)** hERG1 currents registered in control (pLKO.1) and silenced (sh7) cells. Histograms represent the mean \pm s.e.m. (error bars)

control cells transduced with an empty vector (pLKO.1 control versus sh7 silenced cells, Mann-Whitney test, $p < 0.0001$). We did, however, not observe any significant differences in the number of colonies between the control and silenced cells. We also calculated the growth rate of the control and silenced cells during six consecutive days. We found that the proliferation rate of both the sh4 and sh7 cells was lower compared to that of the control cells (Paired t-test, control versus sh7, $p = 0.011$) (Fig. 3d). This reduction in proliferation rate could be explained by a slowdown of the cell cycle, i.e., a delay in S phase entry of the silenced sh7 cells was noted compared to that in control cells (Paired t-test, control versus sh7, $p = 0.031$) (Fig. 3e). Collectively, these experiments indicate that hERG1 silencing has a profound effect in the physiology of HCT116 cells.

Next, we carried out *in vivo* experiments by subcutaneously injecting control and sh7 silenced cells into mice. To this end, 2×10^6 of the respective cells were injected in both flanks of nu/nu mice, after which the developing masses were monitored for

18 days. The tumor masses were measured and compared to those of the control cells 4, 11, 14 and 18 days after inoculation. Overall, we found that the volumes of the masses generated by the silenced cells were significantly smaller compared to those generated by the control cells. The size differences were particularly evident 11 days after inoculation (t-test, $p = 0.041$, DF = 11) (Fig. 3f). We found that hERG1 silencing was maintained until the mice were sacrificed (*hERG1* relative fold change (log fold): pLKO.1 = 0.14 ± 0.04 s.e.m., $n = 6$; sh7 = 0.10 ± 0.03 s.e.m., $n = 7$).

Moreover, we observed by gene expression analysis a strong reduction in the mesenchymal markers and an increment in the epithelial markers tested in the silenced cells (Fig. 3g). We also noted that the actin cytoskeleton of sh7 cells compared to that of the control cells appeared to be disorganized and that focal adhesions to the substratum were rare (Fig. 3h). This altered organization of the cytoskeleton is in conformity with EMT transition [12].

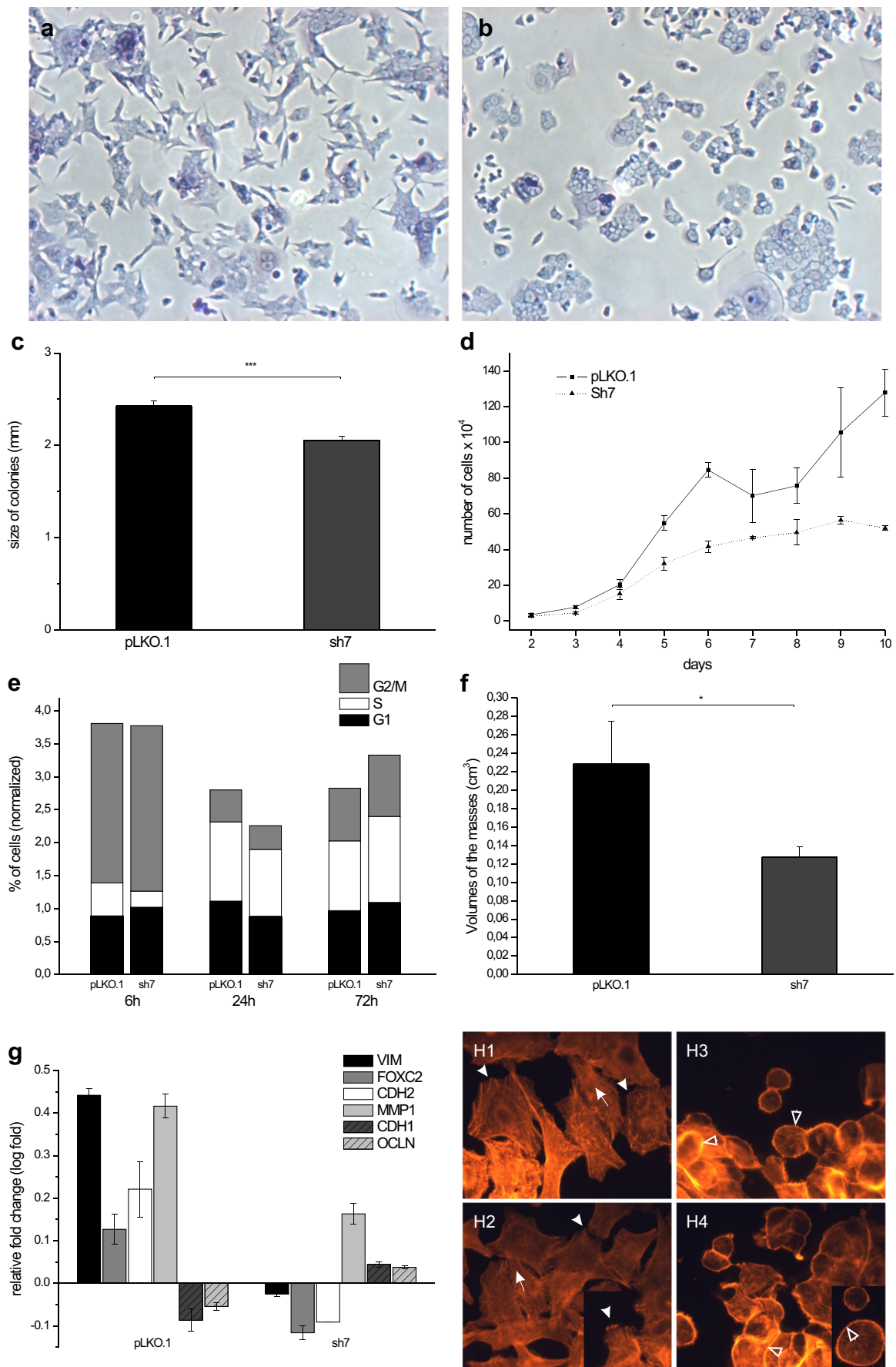


Fig. 3 Morphological and functional characteristics of hERG1 silenced cells. hERG1 silenced cells show different morphologies compared to controls, including a reduced number of membrane protrusions. **(a)** pLKO.1 control cells and **(b)** sh7 silenced cells. **(c)** Soft agar colony formation assay. hERG1 silenced cells form smaller colonies compared to control cells and **(d)** show a reduced proliferative capacity. Histograms represent the mean \pm s.e.m. (error bars). **(e)** Histograms of cell cycle analyses at 6, 30 and 72 h showing a delay in S phase entry of the silenced sh7 cells compared control cells. (S phase: control versus sh7, $p = 0.031$; G2/M phase: control versus sh7, $p = 0.0159$; Paired t-test). **(f)** After subcutaneous injection of control and sh7 silenced cells in nu/nu mice, the volumes of the masses generated by silenced cells were significantly smaller than those of the controls. Histograms represent the mean \pm s.e.m. (error bars) at 11 days after cells injection. **(g)** Expression analysis of mesenchymal (VIM, CDH2, MMP1, FOXC2) and epithelial (CDH1, OCLN) markers. The silenced cells exhibit a stronger epithelial-like molecular profile than the controls (mesenchymal-like profile). Histograms represent the relative fold change \pm s.e.m. (error bars). **(h)** Actin cytoskeleton (red stained) and focal adhesion contacts in control pLKO.1 **(a, b)** and hERG1 silenced sh7 **(c, d)** cells. Control cells show actin stress fibers aligned in the direction of cell migration (arrows), and filopodia and focal adhesions with the substratum (arrow heads). In the silenced cells the actin cytoskeleton is not oriented and the filopodia are strongly reduced. The actin cytoskeleton is mainly localized at the cell surface in the silenced cells (arrow heads not filled). Actin proteins were visualized with rhodamine-conjugated phalloidin. Magnification 1000 \times

3.2 HCT116 cells are resistant to cisplatin treatment

We investigated the response of 4 colorectal cancer-derived cell lines, HCT116, HCT8, HT29 and H630, to cisplatin treatment by flow cytometry using an Annexin-V-FLUOS kit. In order to define suitable drug concentrations, we tested 3 different cisplatin concentrations (50, 100 and 150 μ M) (Fig. 4a). Based on this test, we selected the 100 μ M cisplatin concentration for subsequent experiments (Fig. 4b). By doing so, we noted different apoptotic and necrotic rates in the 4 cell lines, suggesting different sensitivities of the respective cells to cisplatin (Fig. 4). Among the cell lines tested, HCT116 and H630 were more resistant to cisplatin compared to HCT8 and HT29. Interestingly, we found that the silenced HCT116 cells exhibited an increased sensitivity to cisplatin (adherent cells: PLKO.1 (control) mean = 5.2 ± 0.56 s.e.m. versus sh7 (silenced) mean = 9.15 ± 1.88 s.e.m., paired t-test $p < 0.05$; non-adherent cells in the supernatant: PLKO.1 (control) mean = 41.38 ± 3.60 s.e.m. versus sh7 (silenced) mean = 62.68 ± 3.66 s.e.m., paired t-test $p < 0.001$; at 6 different cisplatin concentrations; see materials and methods).

3.3 Riluzole has a synergic effect with cisplatin on HCT116 cells

In order to investigate whether riluzole, a drug that interferes with ion channel activity [31], is able to potentiate the effect of cisplatin in HCT116 cisplatin-resistant cells, we treated these cells with a combination of cisplatin and riluzole. Next, we determined the IC₅₀s of the respective drugs by WST-1 assay

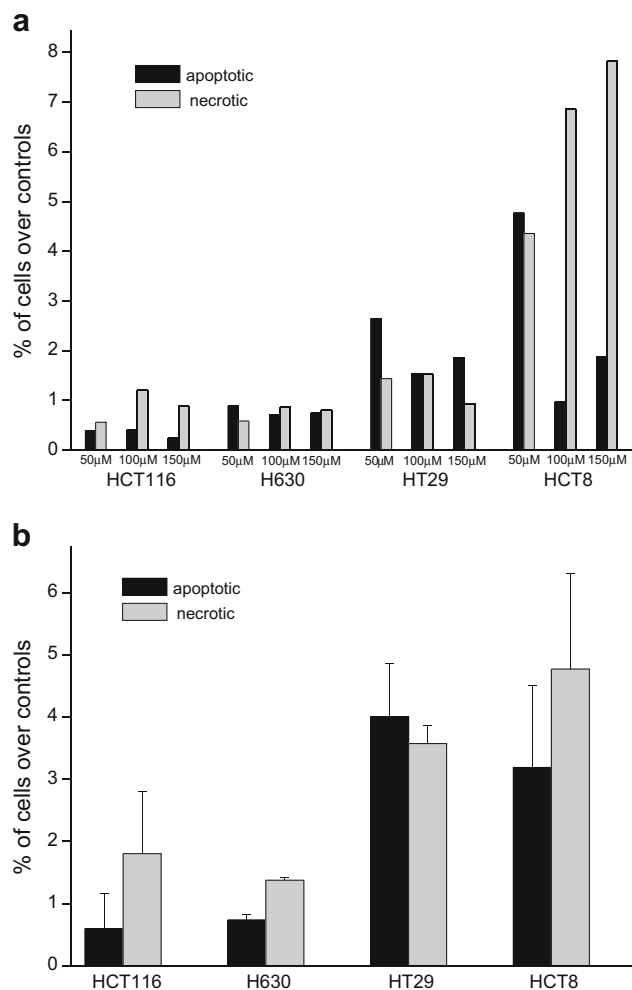


Fig. 4 Apoptotic and necrotic effects of cisplatin on colorectal cancer cells. Colorectal cancer-derived cell lines HCT116, HCT8, HT29 and H630 exhibit different levels of cisplatin sensitivity. **(a)** Dose-response experiment using 3 different concentrations of cisplatin: 50, 100 and 150 μ M. **(b)** HCT116 and H630 cells are relatively resistant to cisplatin (100 μ M concentration), whereas HCT8 and HT29 cells are relatively sensitive (increased apoptosis/necrosis). Apoptosis was measured by Annexin-V staining after a 24-h treatment over untreated control. Error bars represent s.e.m.; data were acquired by flow cytometry

(Fig. 5) and, in order to assess whether riluzole enhances the toxic effect of cisplatin, we exposed the cells to increasing concentrations of cisplatin (1 μ M, 12.5 μ M, 25 μ M, 55 μ M, 85 μ M, 115 μ M) in combination with different constant concentrations of riluzole (10 μ M; 25 μ M; 45 μ M; 65 μ M), including its IC₅₀ value (45 μ M). We found that the toxicity of the drug mixture increased along with the concentration of riluzole (Fig. 6). In addition, we performed a second round of experiments to determine whether cisplatin and riluzole have a synergistic, additive or antagonistic effects using a cell viability assay (WST-1) in conjunction with Calcsyn data analysis. For these experiments, we treated the HCT116 cells with a mixture of cisplatin and riluzole at different concentrations, but a constant

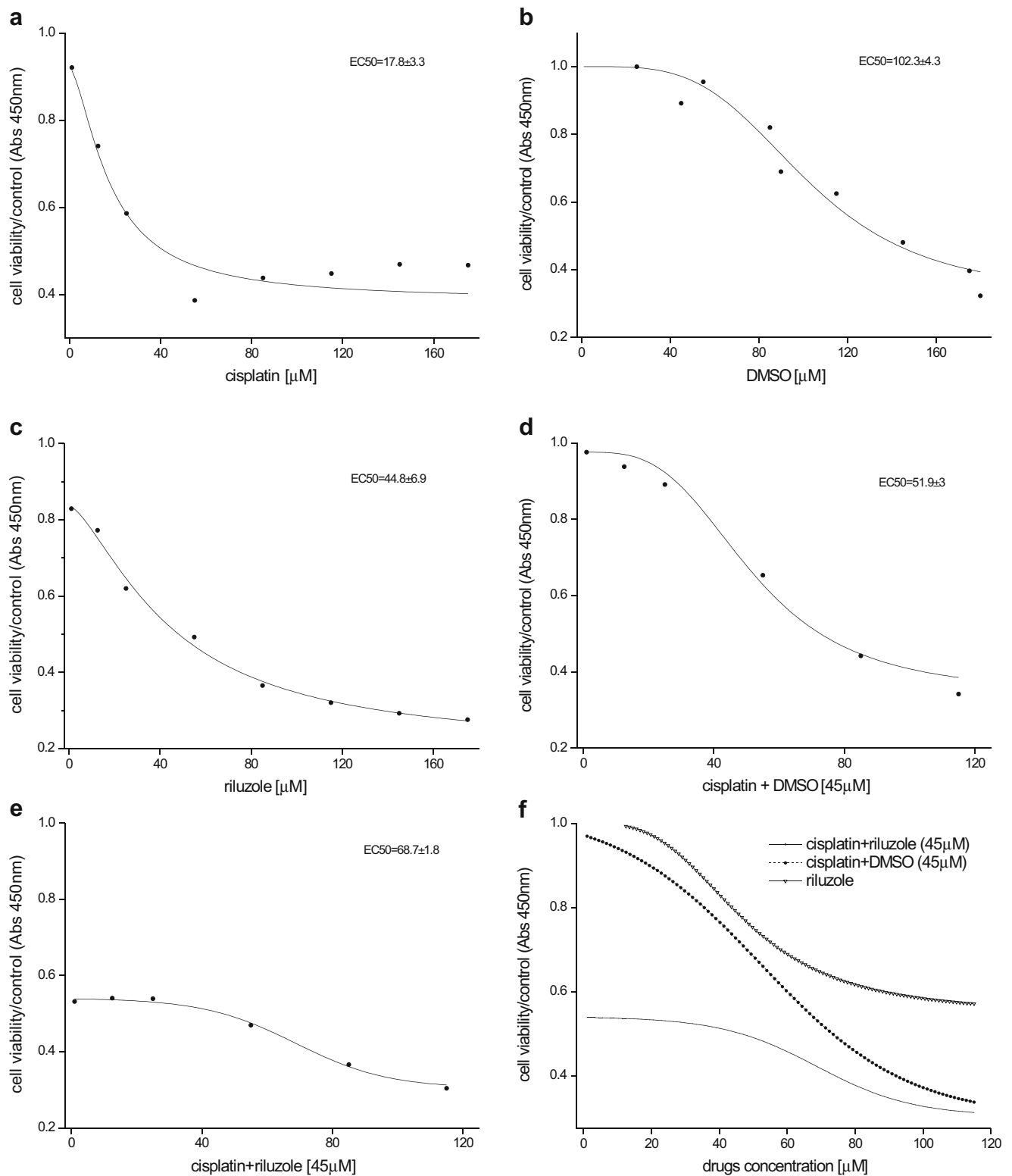


Fig. 5 IC₅₀ measurements. Cells were treated with increasing concentrations of cisplatin (**a**), DMSO (**b**), riluzole (**c**), cisplatin + DMSO (**d**), and cisplatin + riluzole (**e**) to determine the IC₅₀ of each

drug and their combination. (**f**) Toxicity of cisplatin-riluzole mixture. Absorbances were measured using a microplate reader (ELx 800) at a wavelength of 450 nm every 20 min

ratio of the two drugs, with a 2-fold serial dilution of their IC₅₀s (1/2, 1/4, 1/8, 1/16, 1/32, 1/64). By doing so, we found that the

two drugs have synergistic and/or additive effects at low concentrations (Figs. 6 and 7; Table 3S).

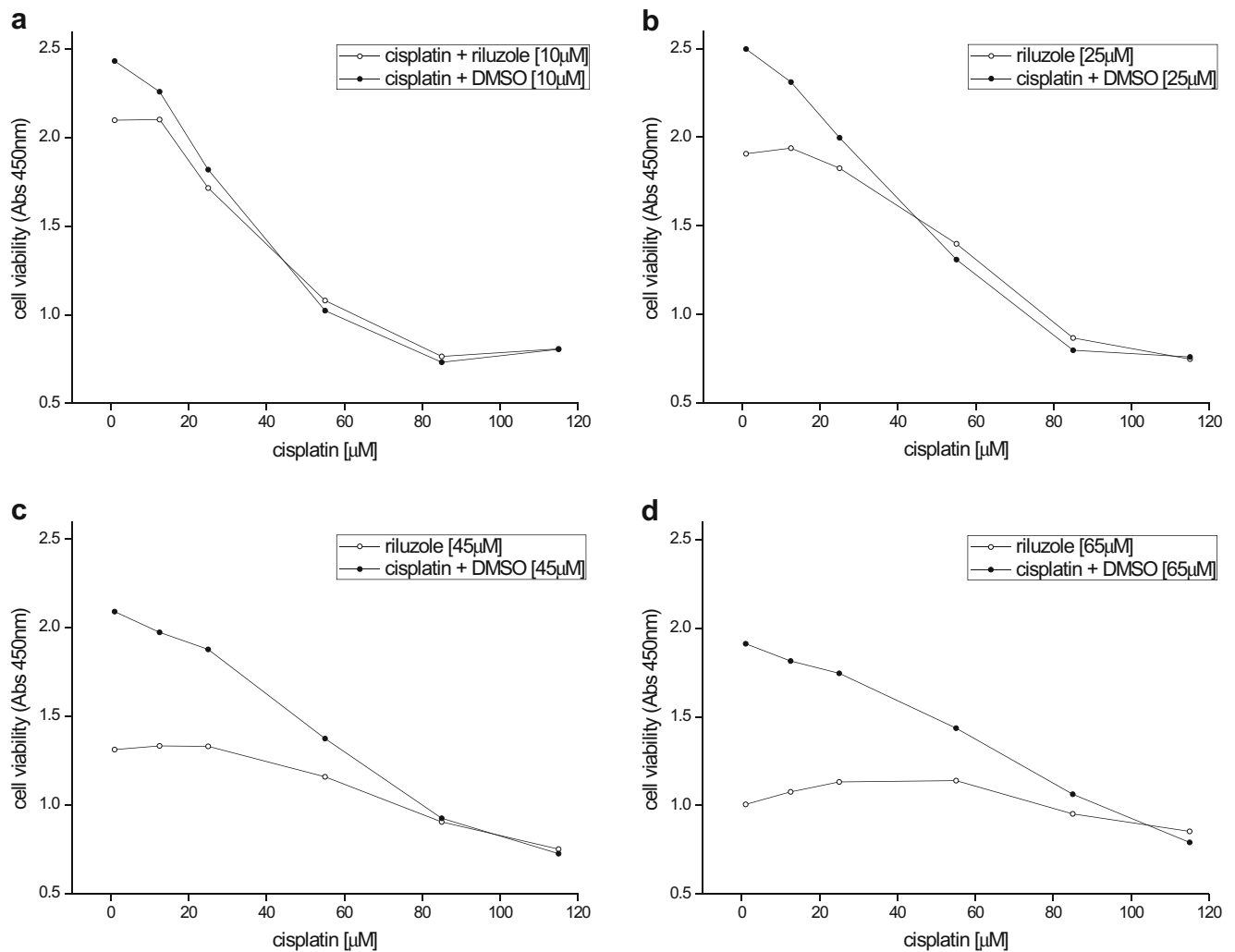


Fig. 6 Concentration-dependent toxicity of cisplatin-riluzole mixture. The toxicity of the cisplatin-riluzole drug mixture increases with the concentration of riluzole. Riluzole concentration: 10 μM (a); 25 μM (b); 45 μM (c); 65 μM (d)

3.4 Calcium-activated potassium channels may serve as riluzole targets in colorectal cancer cells

It has been reported that calcium-activated potassium channel KCa3.1 expression increases the sensitivity of cancer cells to cisplatin [37]. Based on this observation, we set out to investigate the KCa1.1, KCa2.3 and KCa3.1 expression levels in the above mentioned colorectal cancer-derived cell lines. Using qRT-PCR we found that the expression of the corresponding genes varies among these cell lines. KCa3.1 was found to be expressed at the highest level (average Ct values: KCa1.1 = 33.11, KCa2.3 = 30.50, KCa3.1 = 22.17) with log fold ratios of KCa3.1/KCa1.1 = 3.53 and KCa3.1/KCa2.3 = 2.68). We conclude that KCa3.1 is by far the most highly expressed calcium-activated potassium channel. Both HCT116 and H630 cells were found to express KCa3.1 and hERG1 at high levels compared to HCT8 and HT29 cells. In particular, we found that KCa3.1 was notably higher (~6.3 fold) expressed in HCT116 and H630 cells than in HCT8

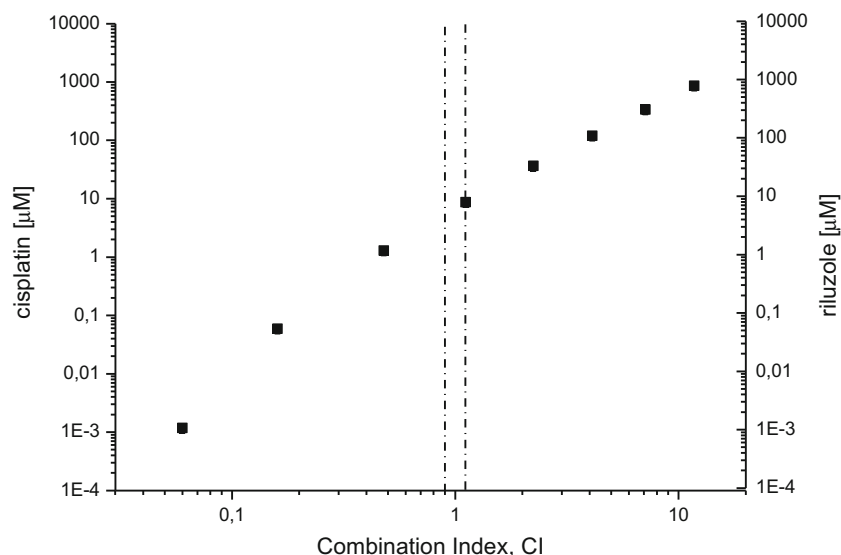
and HT29 cells (Fig. 3S). Thus, KCa3.1 channels may serve as riluzole targets in cisplatin-resistant colorectal cancer cells.

4 Discussion

Epithelium-mesenchymal transition (EMT) plays a key role in tumor progression, and allows cells to invade surrounding tissues, intravasate into lymph and blood vessels ultimately leading to the formation of distant metastases through the activation of complex signaling processes and cytoskeleton rearrangements [38]. Genes involved in EMT regulation have been reported to play a key role in colorectal cancer development [3]. As such, the discovery of novel genes implicated in EMT may be relevant for the clinical management of colorectal cancer.

Here, we found that colorectal cancer-derived HCT116 cells exhibit a mesenchymal molecular profile and, at the same time, a high level of *hERG1* expression [32]. Based on this

Fig. 7 CI simulation of cisplatin-riluzole mixtures using the Calcsyn data analysis tool



observation, we tested the hypothesis that hERG1 channels may be involved in EMT by knocking down its expression in HCT116 cells by lentivirus-mediated RNA interference, which allows a high and stable transduction efficiency (> 70%). We found that hERG1 transcript and protein levels were reduced in the silenced cells and, most importantly, that the silenced cells exhibited reduced hERG1 currents, thereby confirming a functional knockdown and impairment of the hERG1 ion channels. Of the two shRNAs tested, sh4-shRNA was found to elicit a stronger effect on hERG1 expression, whereas sh7-shRNA elicited a stronger phenotypic effect. This discrepancy could be due to the fact that sh4-shRNA recognizes 3 (most abundant) isoforms whereas sh7-shRNA recognizes all known isoforms (Fig. 1S). In fact, the shorter and less abundant hERG1 isoforms orchestrate the correct delivery and assembly of hERG1 channels into the plasma membrane [39]. Nevertheless, we found that both shRNAs were effective in knocking down hERG1 expression, thereby confirming the specificity of the shRNAs selected.

We found that *hERG1* silencing had several consequences, including changes in cell morphology and reductions in the proliferative and tumorigenic capacities of the cells both in vitro and in vivo. The morphological change of the silenced cells, i.e., reductions in lamellipodia and actin rearrangements, are representative reductions in the mesenchymal phenotypes of the cells. In conformity with this notion, we found by gene expression analysis of EMT markers that hERG1 expression knockdown elicited a change in the molecular profile of HCT116 cells in the direction of a more epithelial profile. Moreover, we found that two distinct hERG1 silenced cell lines, sh7-3 and sh7-5, respectively (MOI = 3 and 5) exhibited similar morphologic and molecular profiles, underscoring the experimental reproducibility of the *hERG1* RNAi experiments. An alternative approach used by Restrepo-Angulo et al. [25] to study the involvement of EAG1 channels (closely

related to hERG1) in EMT by inducing EMT in A549 lung cancer cells through TGF β 1 treatment does not directly prove the involvement of EAG1 channels in EMT since TGF β 1 is known to regulate several different biological processes. Our results highlight, for the first time, the role of hERG1 potassium channels in EMT in colorectal cancer cells.

Previous studies have already revealed physical relationships between hERG1 ion channels and proteins involved in cell-cell and cell-substrate interactions, such as integrins [27]. Although integrins alone are not causing cancer, the expression of integrins correlates with cancer progression and a poor patient survival. Notably, oncogenes may require integrin signaling to initiate cancer cell growth and invasion. The availability of compounds capable of targeting hERG1 channels [40] turns the hERG1-integrin complex into an appealing therapeutic target in colorectal cancer, thereby focusing on weakly expressed isoforms in muscle and nervous tissues. Collectively, our data provide indications for a key role of hERG1 in EMT in HCT116 colorectal cancer-derived cells. Additional studies on other (colorectal cancer-derived) cell lines and/or primary tumor samples are required to generalize this finding.

Previous reports have indicated that ion channels may play important roles in tumor progression and treatment. KCa3.1 has, for example, been found to promote apoptosis in human epidermoid cells treated with cisplatin [37]. We found that the silenced hERG1 cells are more sensitive to cisplatin. Therefore, we selected a commercially available drug, riluzole, that is known to act on several different ion channels, i.e., activated KCa1.1, KCa2.3, KCa3.1 and K_{2p}2.1, and blocked KV1, KV3, KV4, Nav1.2, Nav1.4, Nav1.5, Cav1.2 and hERG1 ion channels [31]. In particular, riluzole has been found to reduce the activity of hERG1 ion channels and, at the same time, to stimulate the activity of KCa3.1 ion channels. According to previous studies and our results, modulation of these two ion channels (i.e., decrease hERG1 and increase

KCa3.1 ion channels) should increase the cisplatin sensitivity of cancer cells expressing these genes. Indeed, we found that HCT116 cells overexpressing both hERG1 and KCa3.1, showed an increased sensitivity to cisplatin when treated with riluzole. However, we do not know whether this increased sensitivity is only due to modulation of the hERG1 and KCa3.1 ion channels or whether other channels contribute to this effect as well. Cisplatin is a drug that is widely used in cancer therapy. Cisplatin (and other chemotherapeutic drugs) often face the emergence of resistance, which limits its use. Riluzole could be employed in combination with cisplatin to reduce or delay this resistance. Whereas cisplatin elicits severe neurotoxic effects [41], riluzole has a neuroprotective effect [42, 43]. Therefore, riluzole may alleviate the side effects of cisplatin and prevent resistance to this drug. Since riluzole is FDA approved for use in humans, this could speed up the process of testing this drug combination in clinical trials.

Acknowledgements I would like to thank Annarosa Arcangeli, Massimo D'Amico, Elena Morelli, Serena Pillozzi, Antonella Mannini, Olivia Crociani, Sara Falsini, Luca Gasparoli and Ivo Noci for advice and support.

Compliance with ethical standards

Conflicts of interest The author declares no conflict of interest.

Funding This research did not receive any specific grant from funding agencies in the public, commercial, or not-for-profit sectors and it was partially supported by the University of Florence, Italy.

References

1. J. Guinney, R. Dienstmann, X. Wang, A. de Reynies, A. Schlicker, C. Soneson, L. Marisa, P. Roepman, G. Nyamundanda, P. Angelino, B.M. Bot, J.S. Morris, I.M. Simon, S. Gerster, E. Fessler, E.M.F. De Sousa, E. Missiaglia, H. Ramay, D. Barras, K. Homicsko, D. Maru, G.C. Manyam, B. Broom, V. Boige, B. Perez-Villamil, T. Laderas, R. Salazar, J.W. Gray, D. Hanahan, J. Tabernero, R. Bernards, S.H. Friend, P. Laurent-Puig, J.P. Medema, A. Sadanandam, L. Wessels, M. Delorenzi, S. Kopetz, L. Vermeulen, S. Tejpar, The consensus molecular subtypes of colorectal cancer. *Nat Med* **21**, 1350–1356 (2015)
2. M.M. Hahn, R.M. de Voer, N. Hoogerbrugge, M.J. Ligtenberg, R.P. Kuiper, A.G. van Kessel, The genetic heterogeneity of colorectal cancer predisposition - guidelines for gene discovery. *Cell Oncol* **39**, 491–510 (2016)
3. A. Loboda, M.V. Nebozhyn, J.W. Watters, C.A. Buser, P.M. Shaw, P.S. Huang, L. Van't Veer, R.A. Tollenaar, D.B. Jackson, D. Agrawal, H. Dai, T.J. Yeatman, EMT is the dominant program in human colon cancer. *BMC Med Genet* **4**, 9 (2011)
4. R. Kalluri, R.A. Weinberg, The basics of epithelial-mesenchymal transition. *J Clin Invest* **119**, 1420–1428 (2009)
5. A. Sathyanarayanan, K.S. Chandrasekaran, D. Karunakaran, microRNA-145 modulates epithelial-mesenchymal transition and suppresses proliferation, migration and invasion by targeting SIP1 in human cervical cancer cells. *Cell Oncol* **40**, 119–131 (2017)
6. S. Bugide, V.K. Gonugunta, V. Penugurti, V.L. Malisetty, R.K. Vadlamudi, B. Manavathi, HPIP promotes epithelial-mesenchymal transition and cisplatin resistance in ovarian cancer cells through PI3K/AKT pathway activation. *Cell Oncol* **40**, 133–144 (2017)
7. J.P. Thiery, J.P. Sleeman, Complex networks orchestrate epithelial-mesenchymal transitions. *Nat Rev Mol Cell Biol* **7**, 131–142 (2006)
8. H. Hugo, M.L. Ackland, T. Blick, M.G. Lawrence, J.A. Clements, E.D. Williams, E.W. Thompson, Epithelial-mesenchymal and mesenchymal-epithelial transitions in carcinoma progression. *J Cell Physiol* **213**, 374–383 (2007)
9. B. Baum, J. Settleman, M.P. Quinlan, Transitions between epithelial and mesenchymal states in development and disease. *Semin Cell Dev Biol* **19**, 294–308 (2008)
10. J. Yang, R.A. Weinberg, Epithelial-mesenchymal transition: At the crossroads of development and tumor metastasis. *Dev Cell* **14**, 818–829 (2008)
11. K. Polyak, R.A. Weinberg, Transitions between epithelial and mesenchymal states: Acquisition of malignant and stem cell traits. *Nat Rev Cancer* **9**, 265–273 (2009)
12. S. Corallino, M.G. Malabarba, M. Zobel, P.P. Di Fiore, G. Scita, Epithelial-to-mesenchymal plasticity harnesses endocytic circuitries. *Front Oncol* **5**, 45 (2015)
13. M. Zeisberg, E.G. Neilson, Biomarkers for epithelial-mesenchymal transitions. *J Clin Invest* **119**, 1429–1437 (2009)
14. J.H. Taube, J.I. Herschkowitz, K. Komurov, A.Y. Zhou, S. Gupta, J. Yang, K. Hartwell, T.T. Onder, P.B. Gupta, K.W. Evans, B.G. Hollier, P.T. Ram, E.S. Lander, J.M. Rosen, R.A. Weinberg, S.A. Mani, Core epithelial-to-mesenchymal transition interactome gene-expression signature is associated with claudin-low and metaplastic breast cancer subtypes. *Proc Natl Acad Sci U S A* **107**, 15449–15454 (2010)
15. K. Kunzelmann, Ion channels and cancer. *J Membr Biol* **205**, 159–173 (2005)
16. J.R. Schwarz, C.K. Bauer, Functions of erg K⁺ channels in excitable cells. *J Cell Mol Med* **8**, 22–30 (2004)
17. L.A. Pardo, D. del Camino, A. Sanchez, F. Alves, A. Bruggemann, S. Beckh, W. Stuhmer, Oncogenic potential of EAG K(+) channels. *EMBO J* **18**, 5540–5547 (1999)
18. B. Hemmerlein, R.M. Weseloh, F. Mello de Queiroz, H. Knotgen, A. Sanchez, M.E. Rubio, S. Martin, T. Schliephacke, M. Jenke, R. Heinz Joachim, W. Stuhmer, L.A. Pardo, Overexpression of Eag1 potassium channels in clinical tumours. *Mol Cancer* **5**, 41 (2006)
19. M. Spitzner, J. Ousingsawat, K. Scheidt, K. Kunzelmann, R. Schreiber, Voltage-gated K⁺ channels support proliferation of colonic carcinoma cells. *FASEB J* **21**, 35–44 (2007)
20. A. Litan, S.A. Langhans, Cancer as a channelopathy: Ion channels and pumps in tumor development and progression. *Front Cell Neurosci* **9**, 86 (2015)
21. V.R. Rao, M. Perez-Neut, S. Kaja, S. Gentile, Voltage-gated ion channels in cancer cell proliferation. *Cancers* **7**, 849–875 (2015)
22. S.M. Huber, G.S. Braun, S. Segerer, R.W. Veh, M.F. Horster, Metanephrogenic mesenchyme-to-epithelium transition induces profound expression changes of ion channels. *Am J Physiol Renal Physiol* **279**, F65–F76 (2000)
23. J. Hu, K. Qin, Y. Zhang, J. Gong, N. Li, D. Lv, R. Xiang, X. Tan, Downregulation of transcription factor Oct4 induces an epithelial-to-mesenchymal transition via enhancement of Ca²⁺ influx in breast cancer cells. *Biochem Biophys Res Commun* **411**, 786–791 (2011)
24. F.M. Davis, A.A. Peters, D.M. Grice, P.J. Cabot, M.O. Parat, S.J. Roberts-Thomson, G.R. Monteith, Non-stimulated, agonist-stimulated and store-operated Ca²⁺ influx in MDA-MB-468 breast cancer cells and the effect of EGF-induced EMT on calcium entry. *PLoS One* **7**, e36923 (2012)
25. I. Restrepo-Angulo, C. Sanchez-Torres, J. Camacho, Human EAG1 potassium channels in the epithelial-to-mesenchymal transition in lung cancer cells. *Anticancer Res* **31**, 1265–1270 (2011)

26. A. Schwab, C. Stock, Ion channels and transporters in tumour cell migration and invasion. *Philos Trans R Soc Lond Ser B Biol Sci* **369**, 20130102 (2014)
27. O. Crociani, F. Zanieri, S. Pillozzi, E. Lastraioli, M. Stefanini, A. Fiore, A. Fortunato, M. D'Amico, M. Masselli, E. De Lorenzo, L. Gasparoli, M. Chiu, O. Bussolati, A. Becchetti, A. Arcangeli, hERG1 channels modulate integrin signaling to trigger angiogenesis and tumor progression in colorectal cancer. *Sci Rep* **3**, 3308 (2013)
28. B. Hille, *Ion channels of excitable membranes*, 3rd edn. (Sinauer, Sunderland, Mass, 2001)
29. N.M. Hogan, R.M. Dwyer, M.R. Joyce, M.J. Kerin, Mesenchymal stem cells in the colorectal tumor microenvironment: Recent progress and implications. *Int J Cancer* **131**, 1–7 (2012)
30. J. Lam, N. Coleman, A.L. Garing, H. Wulff, The therapeutic potential of small-conductance KCa2 channels in neurodegenerative and psychiatric diseases. *Expert Opin Ther Targets* **17**, 1203–1220 (2013)
31. A. Sankaranarayanan, G. Raman, C. Busch, T. Schultz, P.I. Zimin, J. Hoyer, R. Kohler, H. Wulff, Naphtho[1,2-d]thiazol-2-ylamine (SKA-31), a new activator of KCa2 and KCa3.1 potassium channels, potentiates the endothelium-derived hyperpolarizing factor response and lowers blood pressure. *Mol Pharmacol* **75**, 281–295 (2009)
32. E. Lastraioli, L. Guasti, O. Crociani, S. Polvani, G. Hofmann, H. Witchel, L. Bencini, M. Calistri, L. Messerini, M. Scatizzi, R. Moretti, E. Wanke, M. Olivotto, G. Mugnai, A. Arcangeli, hERG1 gene and HERG1 protein are overexpressed in colorectal cancers and regulate cell invasion of tumor cells. *Cancer Res* **64**, 606–611 (2004)
33. R. Schonherr, B. Rosati, S. Hehl, V.G. Rao, A. Arcangeli, M. Olivotto, S.H. Heinemann, E. Wanke, Functional role of the slow activation property of ERG K+ channels. *Eur J Neurosci* **11**, 753–760 (1999)
34. M.W. Pfaffl, A new mathematical model for relative quantification in real-time RT-PCR. *Nucleic Acids Res* **29**, e45 (2001)
35. A. Fortunato, L. Gasparoli, S. Falsini, L. Boni, A. Arcangeli, An analytical method for the quantification of hERG1 channel gene expression in human colorectal cancer. *Diagn Mol Pathol* **22**, 215–221 (2013)
36. T.C. Chou, P. Talalay, Theoretical basis, experimental design, and computerized simulation of synergism and antagonism in drug combination studies. *Pharmacol Rev* **58**, 621–681 (2006) Erratum in: *Pharmacol. Rev.* **59**, 124 (2007)
37. E.L. Lee, Y. Hasegawa, T. Shimizu, Y. Okada, IK1 channel activity contributes to cisplatin sensitivity of human epidermoid cancer cells. *Am J Physiol Cell Physiol* **294**, C1398–C1406 (2008)
38. R. Paduch, The role of lymphangiogenesis and angiogenesis in tumor metastasis. *Cell Oncol* **39**, 397–410 (2016)
39. L. Guasti, O. Crociani, E. Redaelli, S. Pillozzi, S. Polvani, M. Masselli, T. Mello, A. Galli, A. Amedei, R.S. Wymore, E. Wanke, A. Arcangeli, Identification of a posttranslational mechanism for the regulation of hERG1 K+ channel expression and hERG1 current density in tumor cells. *Mol Cell Biol* **28**, 5043–5060 (2008)
40. X. Huang, L.Y. Jan, Targeting potassium channels in cancer. *J Cell Biol* **206**, 151–162 (2014)
41. S. Dasari, P.B. Tchounwou, Cisplatin in cancer therapy: Molecular mechanisms of action. *Eur J Pharmacol* **740**, 364–378 (2014)
42. J.W. Albers, V. Chaudhry, G. Cavaletti and R.C. Donehower, Interventions for preventing neuropathy caused by cisplatin and related compounds. *Cochrane Database Syst Rev*, CD005228 (2014)
43. J. Killestein, N.F. Kalkers, C.H. Polman, Glutamate inhibition in MS: The neuroprotective properties of riluzole. *J Neurol Sci* **233**, 113–115 (2005)